Geophys. J. Int. (2011) **187,** 1443–1459 doi: 10.1111/j.1365-246X.2011.05199.x

The 'tsunami earthquake' of 1932 June 22 in Manzanillo, Mexico: seismological study and tsunami simulations

Emile A. Okal[1] and José C. Borrero[2,3]

[1] *Department of Earth and Planetary Sciences, Northwestern University, Evanston, IL 60208, USA. E-mail: emile@earth.northwestern.edu*
[2] *Department of Civil Engineering, University of Southern California, Los Angeles, CA 90089, USA*
[3] *ASR Ltd., 1 Wainui Road, Raglan 3225, New Zealand*

Accepted 2011 August 22. Received 2011 August 12; in original form 2011 February 28

SUMMARY

We conduct a detailed seismological study of the large Colima, Mexico earthquake of 1932 June 3 and of its aftershocks of June 18 and 22. The latter (Event III) generated a tsunami more devastating than that of the main shock despite much smaller seismic magnitudes, thus qualifying as a so-called 'tsunami earthquake'. Relocation based on published arrival times shows that Event III took place up-dip of the main shock. The analysis of the spectral amplitude of mantle surface waves yields low-frequency moments of 24, 5.2 and 4 times 10^{27} dyn cm, respectively, with Event III featuring a moment growing with period, which expresses the source slowness characteristic of 'tsunami earthquakes'. This is confirmed by a deficient energy-to-moment ratio, as derived from high-frequency *P* waves recorded at Pasadena. Near-field hydrodynamic simulations show that the effects of the main shock's tsunami are well modelled by a standard seismic source, whereas the stronger tsunami from Event III can be modelled by rupture along a splay fault in a mechanically deficient material. All our results then fit the model for 'tsunami earthquake' aftershocks proposed for the Kuril Islands by Fukao in 1979.

Key words: Tsunamis; Earthquake source observations; Pacific Ocean.

1 INTRODUCTION AND BACKGROUND

With a published moment of 1.6×10^{28} dyn cm (Okal 1992), the great Colima–Jalisco earthquake of 1932 June 3 was one of the largest to strike Mexico since the dawn of instrumental seismology. It resulted in considerable destruction in the city of Manzanillo and generated a locally damaging tsunami. What makes the event truly remarkable is the occurrence, 19 d later, of an aftershock that generated an even more devastating tsunami, despite a clearly smaller conventional magnitude and seismic moment. This qualifies that aftershock as a so-called 'tsunami earthquake', a class of events defined by Kanamori (1972) as generating tsunamis of much greater amplitude than suggested by their seismic magnitudes, especially conventional ones.

Kanamori's (1972) original paper was based on two events: the 1896 Sanriku earthquake and the 1946 Aleutian one. Later, Fukao (1979) identified the earthquakes of 1963 October 20 and 1975 June 10 in the Kuril Islands as 'tsunami earthquakes'. Both were aftershocks of larger events (on 1963 October 13 and 1973 June 17, respectively) whose tsunamis could be considered as regular. Although Talandier & Okal (1989) further identified the Tonga earthquake of 1982 December 19 as a 'tsunami earthquake', it was not until the decade of the 1990s that interest in this matter was revived due to the occurrence of three events, in Nicaragua (1992 September 02), Java (1994 June 02) and Chimbote, Peru (1996 February 21). More recently, the 2006 Java and 2010 Mentawai earthquakes, both in Indonesia, have qualified as 'tsunami earthquakes'; the latter could be regarded as an aftershock of the 2007 Bengkulu earthquake.

'Tsunami earthquakes' are characterized by a slow rupture, as slow as approximately 1 km s^{-1} (Polet & Kanamori 2000; López & Okal 2006), which leads to a destructive interference of the high-frequency component of their spectrum, expressed, for example, as a strong m_b:M_s anomaly. In turn, such events can be treacherous for the local populations who feel them at most as weak tremors and are thus deprived of a natural warning for the impending tsunami. For example, during the 1992 Nicaragua event ($m_b = 5.3$; $M_s = 7.2$), the earthquake was not felt in some coastal communities, whose unprepared population was washed away 40 min later, at a cost of 170 casualties (Satake *et al.* 1993).

Based on the work of Boatwright & Choy (1986), Newman & Okal (1998) have proposed a modern rendition of the m_b:M_s discriminant, in the form of the parameter $\Theta = \log_{10}(E^E/M_0)$, where E^E is the seismic energy radiated into the body waves, estimated without knowledge of focal mechanism and exact depth, and M_0 the seismic moment. 'Tsunami earthquakes' have parameters Θ typically 1–1.5 logarithmic units below the theoretical value (−4.90) expected from the application of seismic scaling laws.

In general, two tectonic contexts have been proposed for the occurrence of 'tsunami earthquakes'. In Fukao's (1979) model,

they occur on a splay fault developing above the interplate contact into a sedimentary wedge offering inferior mechanical properties and hence a reduced velocity of propagation of the seismic rupture. This model is particularly suited to the case of 'tsunami earthquakes' occurring as aftershocks, where the softer wedge material may have seen a loading by stress transfer from the primary event. Tanioka & Satake (1996) have suggested that it may also apply to the 1896 Sanriku event, where the faulting would have deviated into the wedge at the end of the rupture.

By contrast, in a second scenario, originally described by Tanioka *et al.* (1997), 'tsunami earthquakes' could occur along the interplate contact with the rupture velocities occurring in a sediment-starved environment and expressing a jagged propagation of the rupture along an irregular contact on the shallowest portions of the plate boundary, the absence of a sedimentary plug allowing the up-dip propagation of the rupture to the ocean floor. This scenario would apply in Nicaragua and Java (Polet & Kanamori 2000). In a variation to this model, Bilek & Lay (1999) and Lay & Bilek (2007) have proposed that the slowness of the slip release could be due to the existence of a zone of reduced rigidity along the interplate contact, itself resulting from the ingestion, compaction and dehydration of sediments along its uppermost part. This scenario, which requires a sedimentary input into the subduction zone, could apply to the 2010 Mentawai aftershock of the 2007 Bengkulu earthquake (Newman *et al.* 2011) and possibly to the Hikurangi, New Zealand event of 1947 March 25 (Doser & Webb 2003).

Another mechanism for the generation of exceptionally large tsunamis after earthquakes is the triggering of submarine landslides. Classical examples would include the 1929 Grand Banks, Newfoundland and 1934 Luzon events, for which the existence of the landslides was documented during the repair of telegraphic cables severed by the events (Repetti 1934; Heezen & Ewing 1952). The 1998 tsunami in Papua New Guinea is also generally described as resulting from a landslide triggered by the seismic event with a delay of 13 min (Synolakis *et al.* 2002). Okal & Synolakis (2004) have shown that because landslides and earthquakes obey different scaling laws, their tsunamis feature characteristically different run-up distributions in the near field. Events triggering landslides are generally not considered 'tsunami earthquakes' as their sources do not exhibit seismically anomalous behaviour.

In this general context, the purpose of this paper is to conduct modern seismological studies of the 1932 Manzanillo earthquake series, primarily the main shock (June 3; henceforth Event I), the main aftershock (June 18; Event II) and the 'tsunami earthquake' of June 22 (Event III), and to use their results in hydrodynamic simulations to reproduce the main characteristics of the inundations during the two tsunamis of 1932 June 3 and 22. We conclude that Fukao's (1979) model involving rupture along a splay fault satisfactorily explains the available data.

2 HISTORICAL REPORTS AND PREVIOUS STUDIES

The effects of Events I, II and III and especially of their tsunamis are summarized, for example, by Sánchez & Farreras (1993), based primarily on Mexican newspaper accounts. Event I on 1932 June 3 resulted in severe destruction in Manzanillo and adjoining areas with upwards of 400 casualties. It generated a tsunami featuring a leading depression followed by an inundation with run-up reaching 3 m. Event I was assigned a magnitude $M_{\rm PAS} = 8.1$ by Gutenberg & Richter (1954, hereafter GR). Event II, the largest aftershock on 1932 June 18, caused additional damage, especially in the hinterland locations of Colima and Guadalajara. It generated a minor tsunami starting with a leading depression, but which did not rise over 1 m. GR assigned it $M_{\rm PAS} = 7.9$.

By contrast, Event III, on 1932 June 22, that GR assessed at only $M_{\rm PAS} = 6.9$, generated a catastrophic tsunami that wiped out a 25 km stretch of coastline and in particular, destroyed the resort city of Cuyutlán, killing at least 75 people. Its run-up was reported to have reached 10 m (Sánchez & Farreras 1993), making it clearly larger than that of the main shock and thus qualifying Event III as a 'tsunami earthquake'.

Previous studies of the 1932 earthquakes (Espíndola *et al.* 1981; Wang *et al.* 1982; Eissler & McNally 1984; Singh *et al.* 1984, 1985) had two essential goals: assessing the true sizes of Events I and II (surprisingly enough, Event III generated little interest despite its catastrophic tsunami) and determining their precise epicentres and rupture areas, notably in the framework of their relationship to the Colima earthquake of 1973 and the potential existence of a seismic gap between the two ruptures. The detailed contributions of these previous studies will be described in the relevant sections later. Among their conclusions, Singh *et al.* (1985) suggested the existence of a Colima seismic gap, which was filled during the later Tecoman earthquake of 2003 January 22 (Yagi *et al.* 2004). They also noted that Event I's rupture had to extend across the boundary between the Rivera and Cocos plates, under either Reid's (1976) or Eissler & McNally's (1984) plate geometries, indicating that such boundaries along subduction systems cannot serve as barriers to the rupture of a very large event, an idea later confirmed by Taylor *et al.* (2008) after the 2007 Solomon Islands earthquake.

3 RELOCATION

We relocated systematically the main shock and all 28 apparent aftershocks occurring in 1932, using the data listed by the International Seismological Summary (ISS) and the interactive iterative method of Wysession *et al.* (1991), which includes a Monte Carlo algorithm injecting Gaussian noise into the data set. For events in the 1930s, we give this noise a standard deviation $\sigma_{\rm G} = 5$ s. Results are given in Table 1. None of the relocations could resolve hypocentral depth. In the case of most aftershocks, we used a constrained depth of 25 km, as suggested in the scenario of a large interplate thrust event. We used *S* times only for depleted data sets involving small events, for which their contribution is crucial to the performance of the algorithm.

3.1 The three major events

The relocated epicentre of Event I, at 19.65°N, 104.00°W, is compared on Fig. 1 with various other estimates. The ISS location is shown as a downward triangle at 19.2°N, 104.2°W, whereas GR's is shown as an upward triangle at 19.5°N, 104.25°W. As mentioned by Eissler & McNally (1984), Event I's entry is missing from the collection of B. Gutenberg's notepads (Goodstein *et al.* 1980), so the details of his relocation remain unknown. These authors used Richter's (1958) algorithm based on the variation of *P*-wave residuals with azimuth to derive their own relocation, shown as the square on Fig. 1, at 19.57°N, 104.42°W. Finally, Engdahl & Villaseñor (2002; hereafter EV) relocated the event as part of their Centennial Catalogue, their solution shown on Fig. 1 as the circle, at 19.46°N, 104.15°W. Singh *et al.* (1985) used a combination of differential *S–P* and *L–P* travel times and of first motion polarities at the local

Table 1. Relocations performed in this study.

Number	Date	Origin time (GMT)	Latitude (°N)	Longitude (°W)	Number of stations	σ (s)	Magnitude (M_{PAS})
1 Event I	**3 JUN (155) 1932**	**10:36:52.0**	**19.65**	**104.00**	**73**	**3.87**	**8.1**
2	3 JUN (155) 1932	14:56:24.3	20.40	104.20	5	0.33	
3	3 JUN (155) 1932	15:08:32.1	17.93	104.78	7	3.13	
4	3 JUN (155) 1932	16:28:00.5	18.73	104.21	7	1.90	
5	3 JUN (155) 1932	16:52:36.1	17.94	104.89	5	0.45	
6[a]	3 JUN (155) 1932	17:40:06.9	19.44	104.35	25	4.27	6
7	3 JUN (155) 1932	20:00:07.6	20.38	105.74	4	1.37	
8	3 JUN (155) 1932	20:12:30.3	22.93	103.81	9	2.09	
9	4 JUN (156) 1932	19:01:24.6	18.47	104.93	9	1.02	
10[a]	4 JUN (156) 1932	21:39:29.5	19.25	105.39	15	3.30	
11[a]	5 JUN (157) 1932	09:04:43.1	19.29	105.06	27	3.19	$6\,^{1}/_{4}$
12	8 JUN (160) 1932	10:36:56.8	18.90	104.74	10	2.79	
13[a]	9 JUN (161) 1932	04:35:38.7	18.91	104.99	25	3.93	
14 Event II	**18 JUN (170) 1932**	**10:12:13.1**	**19.58**	**103.84**	**56**	**3.73**	**7.9**
15	18 JUN (170) 1932	21:59:04.2	17.45	103.12	10	3.45	
16	19 JUN (171) 1932	08:41:28.8	18.04	104.37	9	3.60	
17 Event III	**22 JUN (174) 1932**	**12:59:29.3**	**19.24**	**104.34**	**57**	**3.81**	**6.9**
18	22 JUN (174) 1932	16:48:33.8	19.53	105.01	7	4.03	
19	25 JUN (177) 1932	20:54:15.6	18.36	104.4	8	2.36	
20	5 JUL (187) 1932	10:06:23.7	17.25	104.44	6	0.70	
21	12 JUL (194) 1932	13:52:05.6	16.10	102.63	7	2.47	
22[a]	25 JUL (207) 1932	09:12:50.3	18.96	104.01	71	2.67	$6\,^{3}/_{4}$
23[b]	24 AUG (237) 1932	03:40:25.1	18.50	105.17	12	3.14	
24[a]	8 SEP (252) 1932	01:41:14.1	19.33	103.90	30	2.17	
25	29 OCT (303) 1932	03:36:49.9	19.25	105.48	16	4.56	
26[a]	17 NOV (322) 1932	06:02:59.3	19.27	103.79	39	2.86	$6\,^{1}/_{4}$
27	19 NOV (324) 1932	08:58:48.8	18.47	105.24	10	3.13	
28[a]	7 DEC (342) 1932	16:22:14.1	19.02	104.05	59	2.47	$6\,^{1}/_{2}$
29	20 DEC (355) 1932	02:39:29.0	19.97	105.58	10	2.95	

[a]Major, well-located aftershock, shown as solid dot on Fig. 2.
[b]Probable outer rise event, shown as square (with dotted confidence ellipse) on Fig. 2.

station MNZ and the regional stations GUM and TAC (Tacubaya), in support of Eissler & McNally's (1984) solution. We note that both GR's and EV's locations fall within our Monte Carlo confidence ellipse.

Fig. 1 also shows our relocation of Event II, at 19.58°N, 103.84°W, as well as the other estimates for this source. Note that the ISS did not locate the event, but simply assumed a common epicentre with Event I. There is generally more scatter among the published solutions, but once again our confidence ellipse includes EV's solution and grazes GR's.

In the case of Event III, all solutions are displaced SSW from the main shock in the vicinity of our relocated solution (19.24°N, 104.34°W), although our confidence ellipses for the three events do intersect. However, we emphasize the trend, common to all solutions, in the relative locations of Events III and I. Modern relocations show Event III 48 km from Event I in the azimuth N207°E (EV) or 52 km in the azimuth N219°E (this study). Even the ISS and GR's locations (constrained to precisions no better than 0.1° and 1/4°, respectively) exhibit similar trends (33 km, N250°E and 55 km, N205°E, respectively). All this evidence strongly suggests that Event III occurred about 50 km seawards of the main shock, in a geometry which would be compatible with rupturing either at the very top of the interplate contact, or along a splay fault located in an accretionary wedge inside the North American Plate.

3.2 Other aftershocks

Among the 29 earthquakes listed on Table 1, we earmark with a [a] eight events which have generally better locations, as evidenced by smaller confidence ellipses. Five of those were assigned magnitudes $M_{PAS} \geq 6$ by GR. Those eight 'major' aftershocks are plotted with their confidence ellipses on Fig. 2 and can be used to obtain an estimate of the length of rupture of the main shock, their relocated epicentres spreading over 140 km parallel to the coastline. This estimate is half the 280 km proposed by Singh *et al.* (1984). We note that these authors did not carry out a full relocation based on worldwide travel times but rather used a limited number of differential times, such as *S–P* at regional distances. On their Fig. 2, the resulting estimate for the fault length relies entirely on their events 1, 22 and 12. The former two are not reported by the ISS and thus cannot be independently relocated. The latter is our Event 23 (1932 August 24; [b] in Table 1), which clearly occurred farther south and east with a moderate-sized confidence ellipse, not reaching the coastline. We interpret this as an outer-rise intraplate event, which we exclude from the data set of genuine aftershocks defining the extent of rupture. The remainder of Singh *et al.*'s (1984) aftershock distribution extends over approximately 150 km (their fig. 2) in general agreement with our estimate of 140 km.

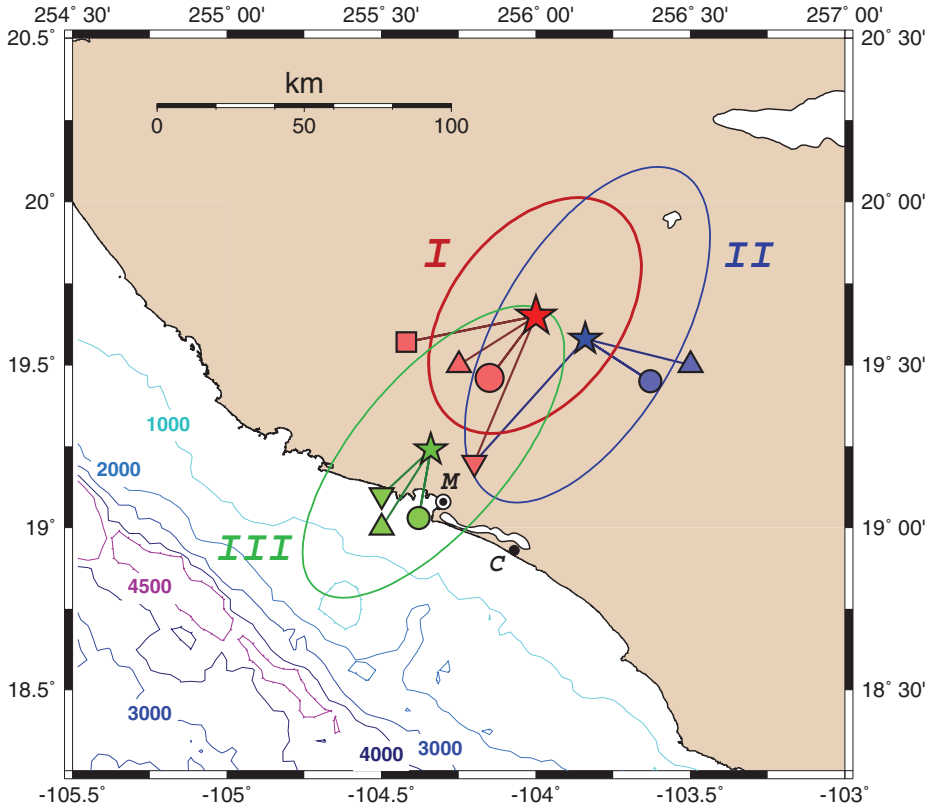

Figure 1. Relocation of Events I (red), II (blue) and III (green). For each event, our relocated epicentre is shown as the large star (surrounded by its Monte Carlo confidence ellipse), the ISS location as the inverted triangle, GR's estimate as the upward triangle, EV's relocation as the circle and in the case of Event I, Eissler & McNally's (1984) estimate as the square. Note that Event III is systematically offset about 50 km to the SSW of Event I. The bull's eye symbol (M) identifies the city of Manzanillo and the solid dot (C) the resort of Cuyutlán. Isobaths are drawn every 1000 m, with the exception of the deepest one (4500 m).

4 WAVEFORM STUDIES

We were able to gather a number of historical seismograms of Events I, II and III for the purpose of computing spectral amplitudes of long-period surface waves and examining the energy contained in teleseismic *P* waves. Unfortunately, we faced a number of challenges due to the date of the events (predating, e.g. the development of H. Benioff's broad-band '1–90' seismometers), the significant difference in size between Events I and III (which can preclude a direct comparison, with Event III hardly emerging from the noise on Wiechert seismograms), and other unfortunate occurrences (the records being changed or the presence of obvious non-linearities). Table 2 lists all the records used in this study.

4.1 Mantle waves: seismic moments and low-frequency spectrum

For each available surface wave, we compute spectral amplitudes at mantle periods ($50 \leq T \leq 250$ s), which we interpret as mantle magnitudes $M_{\rm m}$ in the formalism of Okal & Talandier (1989). Unfortunately, the resulting data sets are insufficient to allow a formal inversion, for example, using the Preliminary Determination of Focal Mechanism (PDFM) algorithm (Okal & Reymond 2003). Under the circumstances, we assume for Events I and II a mechanism ($\varphi = 310^\circ$; $\delta = 14^\circ$; $\lambda = 90^\circ$) expressing pure subduction along the local plate boundary; this mechanism is also very close to that of the nearby Colima earthquake of 2003 January 22 ($\varphi = 308^\circ$; $\delta = 12^\circ$; $\lambda = 110^\circ$). For Event III, we assume a steeper dip, representative of faulting along a splay fault in the accretionary wedge that will be our preferred model. However, a mechanism similar to those used for Events I and II would not modify our main conclusion, namely that Event III features source slowness.

We use these geometries to compute focal mechanism corrections to our $M_{\rm m}$ values, which then become corrected magnitudes $M_{\rm c}$ (Okal & Talandier 1989) and can be interpreted in terms of a seismic moment (in dyn cm):

$$\log_{10} M_0 = M_c + 20. \quad (1)$$

Fig. 3 regroups our results for all three events. We find an average value $M_{\rm c} = 8.19 \pm 0.36$ for Event I, corresponding to $M_0 = 1.55 \times 10^{28}$ dyn cm, in excellent agreement with our one-station estimate (Okal 1992). There is a slight growth of moment with period due to the effect of source finiteness at higher frequencies (Ben-Menahem 1961) with an average value of 2.4×10^{28} dyn cm beyond 150 s that we propose as the static value of M_0 for Event I. Note that a regression of the full data set of $M_{\rm c}$ values with frequency, shown as the blue dashed line on Fig. 3, does not stray outside of the 2σ window shown as the yellow band.

Previous determinations of Event I's moment include Espíndola *et al.*'s (1981) comparative study of surface waves at Uppsala in the 40–70 s range (1.0×10^{28} dyn cm), Wang *et al.*'s (1982) analysis of 50-s surface waves at three European stations (0.9×10^{28} dyn cm) and Singh *et al.*'s (1984) body wave modelling at Uppsala and Stuttgart (0.3×10^{28} dyn cm).

All these figures are substantially lower than ours, and expectedly so, because the authors worked at higher frequencies, which for this size of source are systematically affected by the destructive

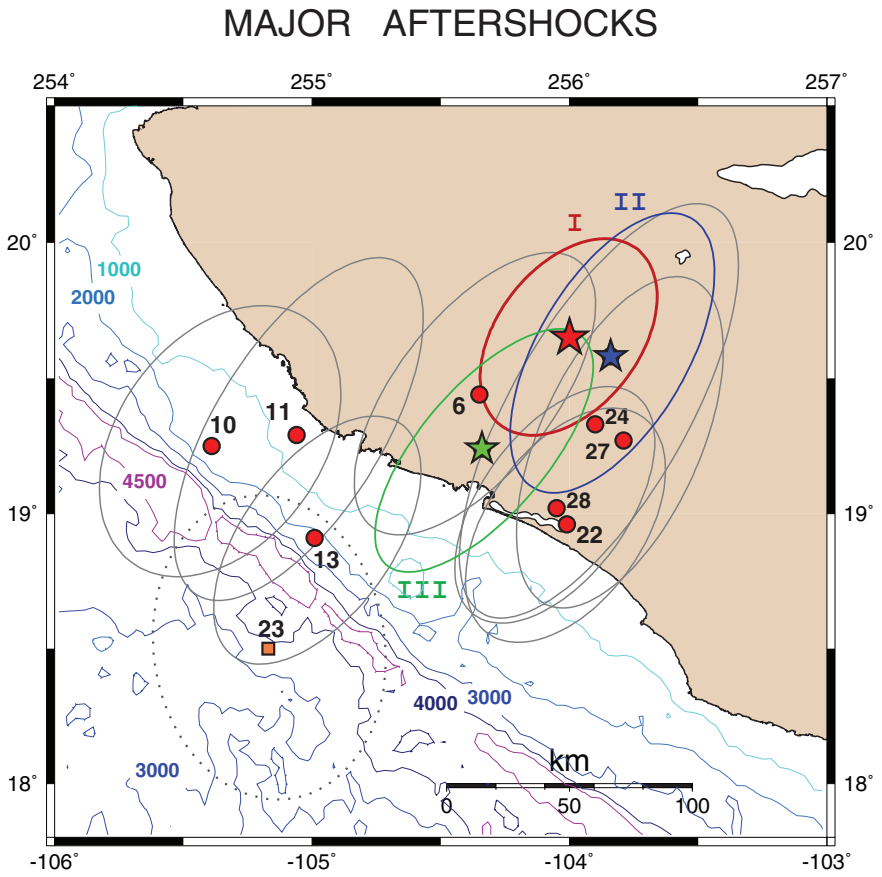

Figure 2. Relocation of the principal aftershocks, flagged with a [a] in Table 1. These events have relatively small confidence ellipses and as such help provide an estimate of the dimension of rupture. Numbers refer to Table 1. Isobaths identify the location of the trench and suggest that Event 23 (square, with dotted ellipse), flagged with a [b] in Table 1, is an outer rise earthquake.

interference due to source finiteness (Ben-Menahem 1961; Geller 1976).

In the case of Event II, we could find only one set of usable records, at DBN, which are however excellent and offer a perfectly flat moment featuring no trend with period and yielding $M_0 = 5.2 \times 10^{27}$ dyn cm. This value remains greater than Singh *et al.*'s (1984) estimate from body waves (2.1×10^{27} dyn cm) but surprisingly, smaller than Wang *et al.*'s (1982) (7.3×10^{27} dyn cm).

The most interesting results are, of course, those for Event III for which, to our best knowledge, no prior computation of seismic moment was reported in the literature. As shown on Fig. 3, M_0 increases regularly and steeply with period on all three available records, gaining close to a factor of 10 between 80 and 200 s. Our empirical regression features a slope of -13.7 logarithmic units per mHz, 2.5 times steeper than for Event I, and clearly shows that the data set transgresses its 2σ band. This suggests that Event III has a static moment of approximately 4×10^{27} dyn cm and definitely identifies it as an event featuring an anomalously slow source, confirming its nature as a 'tsunami earthquake'. Its relationship to the main shock fits Fukao's (1979) model and is particularly reminiscent of that of the Kuril duo on 1963 October 13 and 20.

4.2 Energy-to-moment ratios and parameters Θ

The slow character of a seismic source, such as a 'tsunami earthquake', can also be assessed by comparing the high- and low-frequency parts of its source spectrum. Following the work of Newman & Okal (1998), itself based on Boatwright & Choy (1986), we seek to obtain slowness parameters $\Theta = \log_{10}(E^{\mathrm{E}}/M_0)$ for Events I, II and III. Okal & Kirby (2002) and later López & Okal (2006) have shown that this approach can be applied to paper records from historical events. In the case of the 1932

Table 2. Seismic records used in this study. Epicentral distances are computed for Event I and rounded to the nearest degree.

Station		Distance	Instrument		Event(s) studied	Wave trains used
Name	Code	(°)	Type	Component		
De Bilt, the Netherlands	DBN	86	Galitzin	NS	I	G_1
De Bilt, the Netherlands	DBN	86	Galitzin	EW	I, II, III	R_1
Pasadena, California	PAS	19	Wood–Anderson	WE	I, II, III	P
Saint Louis, Missouri	SLM	23	Wiechert	NS	I	R_1
San Juan, Puerto Rico	SJG	36	Wenner	EW	III	R_1
Uppsala, Sweden	UPP	88	Wiechert	EW	I	R_1

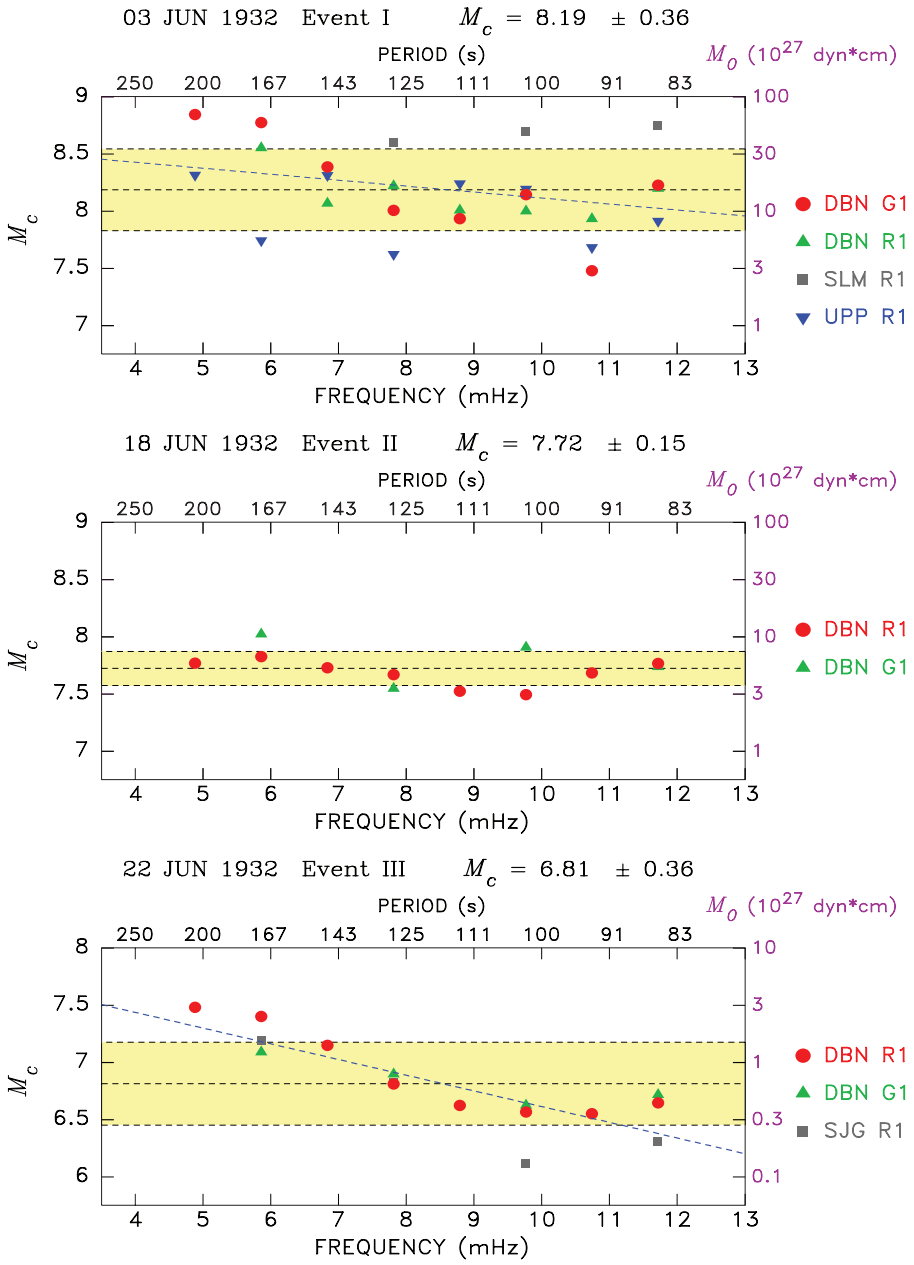

Figure 3. Mantle magnitude analysis of the low-frequency surface waves from Events I, II and III. For each event, the values of M_c, the mantle magnitude corrected for focal mechanism (Okal & Talandier 1989), are plotted against frequency, with relevant period and moment scales given along the top and right axes. The central dashed line and shaded area are the average value and 2σ confidence interval, respectively. For Events I and III, the oblique dashed lines are linear regressions of the data sets. Note the flat spectrum of Event II and the mild frequency dependence for Event I expressing source finiteness. In the case of Event III, the strong slope, reaching outside of the confidence interval, expresses the intrinsic slowness of the source.

Mexican series, we are limited by the availability of adequate records, in particular because the events predate the development of the broad-band '1–90' instruments (available at Pasadena starting in 1937).

We were able to gather on-scale records of the generalized P waves from all three events on the east–west Wood–Anderson seismometer at Pasadena (Fig. 4). These records were digitized at a sampling rate $t = 0.1$ s and processed through the standard algorithm for the computation of Θ. A correction is introduced to take into account the use of a single horizontal component. Because the epicentral distances involved (19.17°, 19.32° and 19.30°, respectively) are significantly shorter than the range of applicability ($35° \leq \Delta \leq 80°$) of the distance correction used in the definition of Θ (Newman & Okal 1998), we use an empirical extension of this correction derived by Ebeling & Okal (2007). We obtain $\Theta = -5.20$, -5.14 and -6.18, respectively for Events I, II and III. We emphasize that, because Ebeling & Okal's (2007) regional distance corrections were derived empirically in the absence of a rigorous theoretical framework, these values remain tentative in an absolute sense; however, because the epicentral distance is essentially the same for all three earthquakes, the relative values for the three events are robust. Notwithstanding this reservation, Fig. 5 shows that Events I and II feature Θ values characteristic of large interplate thrust earthquakes whereas Event III exhibits an energy-to-moment

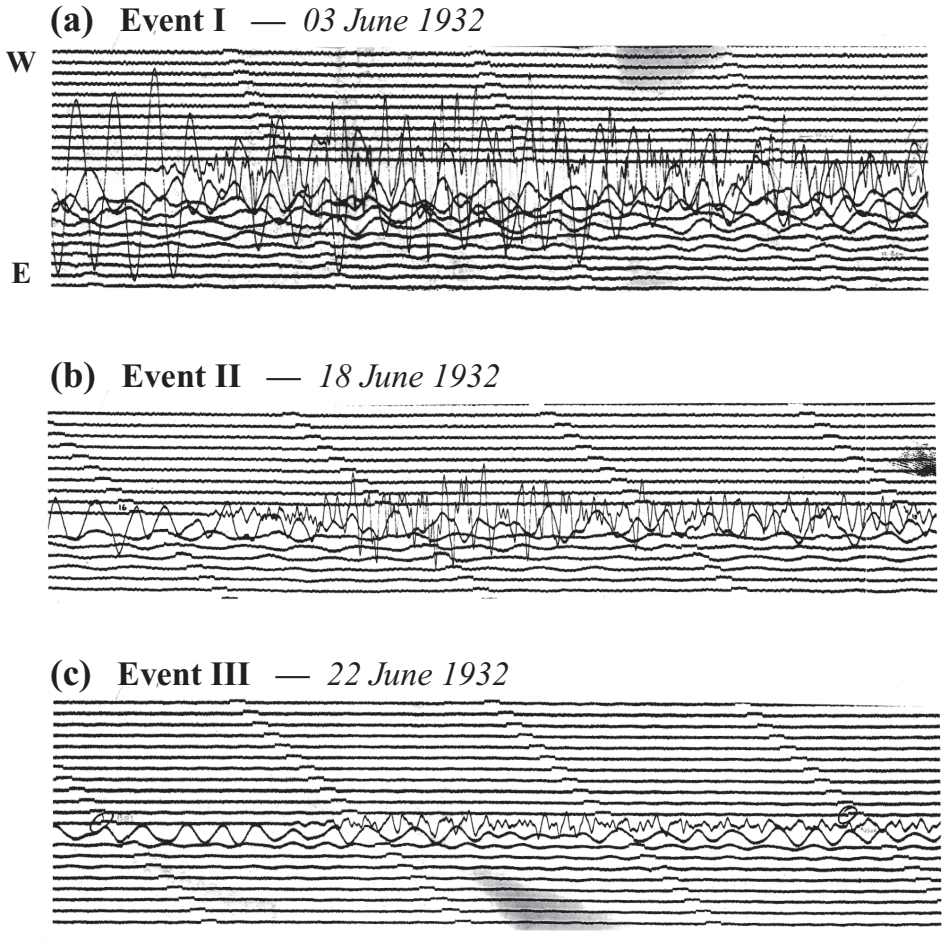

Figure 4. Records of Events I, II and III on the west–east component of the 6-s Wood–Anderson torsion seismometer at Pasadena. The common scale allows for direct comparison of the three events, clearly exposing Event III's deficiency in high frequencies. Tick marks indicate minutes.

ratio typical of 'tsunami earthquakes' such as the 1992 Nicaragua event.

5 TSUNAMI SIMULATIONS

5.1 Methodology

In this section, we simulate the regional tsunamis generated by Events I, II and III based on models of their ruptures derived from the waveform studies of Section 4. For each event, we use scaling laws (Geller 1976) to interpret the static values of the seismic moment M_0 in terms of fault length L, fault width W and seismic slip Δu. All relevant parameters are listed in Table 3. We use Mansinha & Smylie's (1971) algorithm to compute the field of static displacement of the ocean bottom resulting from the dislocation, which is then taken as the initial condition, for the numerical simulation, of the deformation of the sea surface. This approximation, classical in tsunami modelling, is justified by the fact that any seismic rupture, including a slow one characteristic of a 'tsunami earthquake', remains hypersonic with respect to the propagation velocities of tsunamis (Okal & Synolakis 2003). The simulation uses the Method of Splitting Tsunamis (MOST) code (Titov & Synolakis 1998) that solves the full non-linear equations of hydrodynamics under the shallow-water approximation by finite differences and through the method of alternate steps (Godunov 1959). MOST has been extensively validated through comparisons with laboratory and field data, per standard international protocols; full details can be found in Synolakis (2003). Simulations are carried out for a time window lasting 2 hr after origin time.

The present computations use three nested grids, the coarsest one covering a total area of 330 000 km^2 and the finest one, shown on Figs 6–11, featuring a sampling of 0.1 nautical mile (0.185 km). All bathymetry grids are derived from the GEBCO 0.5-min global data set, the finer ones being simply interpolated from the coarser grid. This procedure is necessary to allow a run-up computation simulating the interaction with the coastline. As a result, our simulations remain tentative in an absolute sense, but can be used to compare the relative responses of the coastline to different seismic source scenarios. The time steps are adjusted for each grid, down to $t = 1$ s for the finest one, to satisfy the stability condition of Courant *et al.* (1928).

5.2 Event I: 1932 June 03

In the first model tested for the main shock, labelled 03.1, we derive a centroid of the rupture by assuming that our relocated epicentral location corresponds to the initiation of the rupture at the deepest boundary of the faulting area. The parameters $L = 150$ km, $W = 75$ km and $\Delta u = 4.5$ m are derived from scaling laws (Geller 1976). Note that the fault length is in good agreement with the

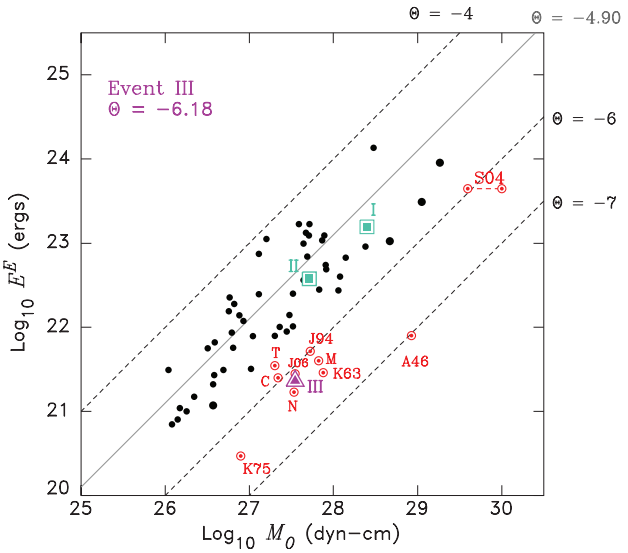

Figure 5. Summary of energy-to-moment ratios for a data set of large recent earthquakes (adapted from Newman & Okal 1998; López & Okal 2006; Okal *et al*. 2011). For each event, the estimated energy E^E is plotted against the seismic moment M_0 in logarithmic units. The diagonal lines feature constant Θ, the solid one being the theoretical value (−4.90) expected from scaling laws. Solid dots form a background of typical values from recent sources. Bull's eye symbols denote 'tsunami earthquakes', all featuring $\Theta \leq -5.8$ (N: Nicaragua, 1992; J: Java, 1994 and 2006; M: Mentawai, 2010; K: Kuril, 1963 and 1975; C: Chimbote, Peru, 1996; T: Tonga, 1982; A46: Aleutian, 1946; S04: Sumatra, 2004; for the latter, both the CMT and normal mode moments are shown). The 1932 events are shown as the squares (Events I and II, regular Θ) and the triangle (Event III, deficient Θ; 'tsunami earthquake').

extent of the well-located aftershocks plotted on Fig. 2. The resulting displacement field is shown on Fig. 6(a) and a close-up of the wave heights in Manzanillo and its vicinity on Fig. 6(b). Our results show maximum amplitudes on the order of 3.5 m in the bay of MNZ, in general agreement with the descriptions compiled by Sánchez & Farreras (1993), and lesser values in Cuyutlán.

We also explored, in Model 03.2, the possibility of a source displaced WNW along the coastline, as suggested by Singh *et al.*'s (1985) model of an extended rupture and Eissler & McNally's (1984) relocation significantly westwards of the other solutions (Fig. 1). Fig. 7 shows that the simulated tsunami amplitude falls to 1.5 m in Manzanillo, substantially lower than observed. In summary, Model 03.1 best describes the effects of the tsunami on Manzanillo and its vicinity.

5.3 Event II: 1932 June 18

As expected, the combination of a smaller source and an inland epicentre (as confirmed by significant destruction in the hinterland) results in a much smaller tsunami with simulated amplitudes around Manzanillo of 1–1.5 m (Fig. 8), once again in agreement with the reported values (Sánchez & Farreras 1993).

5.4 Event III: 1932 June 22

Having assessed in Section 4 the static moment of Event III at 4×10^{27} dyn cm, we explore several possible geometries for its source. In Model 22.1, we consider the case of a regular earthquake, obeying scaling laws, but simply located up-dip from the main shock. Although its location on the interplate contact would be generally similar to that of the 2010 Mentawai, Sumatra 'tsunami earthquake' (Newman *et al.* 2011), we keep a conventional rigidity for this model. Fig. 9 shows that the wave heights remain moderate, not exceeding 2.5–3 m in the area of Manzanillo and Cuyutlán. In short, this model simulates a tsunami smaller than that of Event I and thus, fails to account for the much larger wave heights observed.

In Model 22.2, we consider a rupture on a splay fault, by changing the dip to 45° whereas maintaining all other parameters, including the rigidity, unchanged. Fig. 10 shows that the results are changed only marginally and that it would not predict the reported widespread inundation.

Scenario 22.3 is inspired by Lay & Bilek's (2007) model of a variable, generally deficient, rigidity along the uppermost part of the subduction interplate. It shares the focal geometry of Model 22.1, but features a lower rigidity, and hence an enhanced slip, with a slightly elongated more 'ribbon-like' fault geometry. As shown on Fig. 11, the maximum run-up increases to 4 m in Manzanillo and 4.5 m in Cuyutlán but remains smaller than reported (note that the color palette used on Figs 11 and 12 differs from that of Figs 6–10).

Then, in Model 22.4, we keep the focal mechanism of the splay fault in Model 22.2, but release it in a sedimentary material featuring a deficient rigidity. This is the exact geometry favoured by Fukao (1979) to explain the Kuril 'tsunami earthquakes' of 1963 October 20 and 1975 June 10. The vertical static displacement from the earthquake grows to a maximum of 3.2 m (Fig. 12a) and wave heights reach 7 m (Fig. 12b). We also show, on Fig. 12(c), run-up at selected locations along the coastline obtained, on initially dry land, as the elevation above sea level of the point of maximum wave inundation. Run-up reaches 7 m in the bay of Manzanillo and 6–7 m further east in Cuyutlán. Also, Fig. 12(b) shows inundation of the land spit separating the ocean from the Cuyutlán lagoons, in

Table 3. Parameters of rupture models used in tsunami simulations.

	Centroid of rupture		Depth to top of rupture (km)	Focal mechanism			Rupture parameters			Rigidity,	Moment,
Name	°N	°E		φ (°)	δ (°)	λ (°)	L (km)	W (km)	Δu (m)	μ (dyn cm^{-2})	M_0 (dyn cm)
Event I: 1932 June 3											
03.1	19.06	−104.37	20	304	15	90	150	75	4.5	5×10^{11}	2.5×10^{28}
03.2	19.56	−105.16	20	304	15	90	150	75	4.5	5×10^{11}	2.5×10^{28}
Event II: 1932 June 18											
18.1	19.28	−104.21	20	304	15	90	88	44	2.6	5×10^{11}	5×10^{27}
Event III: 1932 June 22											
22.1	18.7	−104.26	10	304	15	90	82	41	2.4	5×10^{11}	4×10^{27}
22.2	18.66	−104.29	10	304	45	90	82	41	2.4	5×10^{11}	4×10^{27}
22.3	18.66	−104.26	10	304	15	90	100	40	4	2.5×10^{11}	4×10^{27}
22.4	18.66	−104.29	10	304	45	90	86	41	6.5	1.8×10^{11}	4×10^{27}

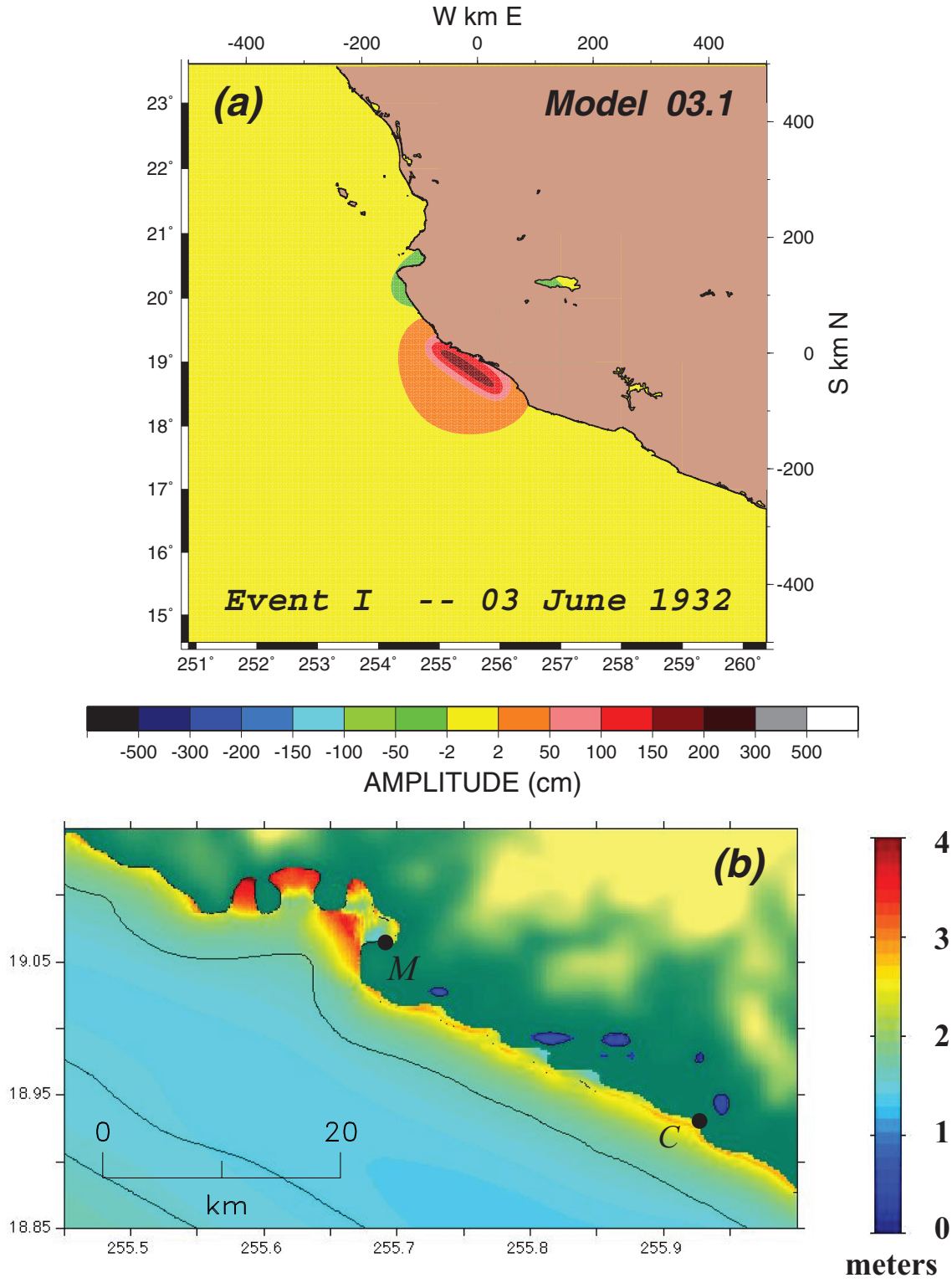

Figure 6. Simulation of Event I's tsunami under Model 03.1. (a) Field of vertical displacement of the ocean floor, computed using Mansinha & Smylie's (1971) algorithm. (b) Field of maximum wave heights during a 2-hr time window after origin time.

accordance with the description reported in local newspapers (El Excelsior 1932) and summarized by Sánchez & Farreras (1993).

The significant difference in wave height and run-up between Models 22.2, 22.3 and 22.4 constitutes a numerical illustration of Okal's (1988) theoretical results, showing that rupture in a 'sedimentary' layer, that is, a structure with deficient rigidity, enhances the excitation of tsunamis relative to seismic surface waves, especially for a 45°-thrust geometry, thereby explaining the properties of 'tsunami earthquakes' under Fukao's (1979) model. Finally, note that even the maximum run-up reported (but not scientifically

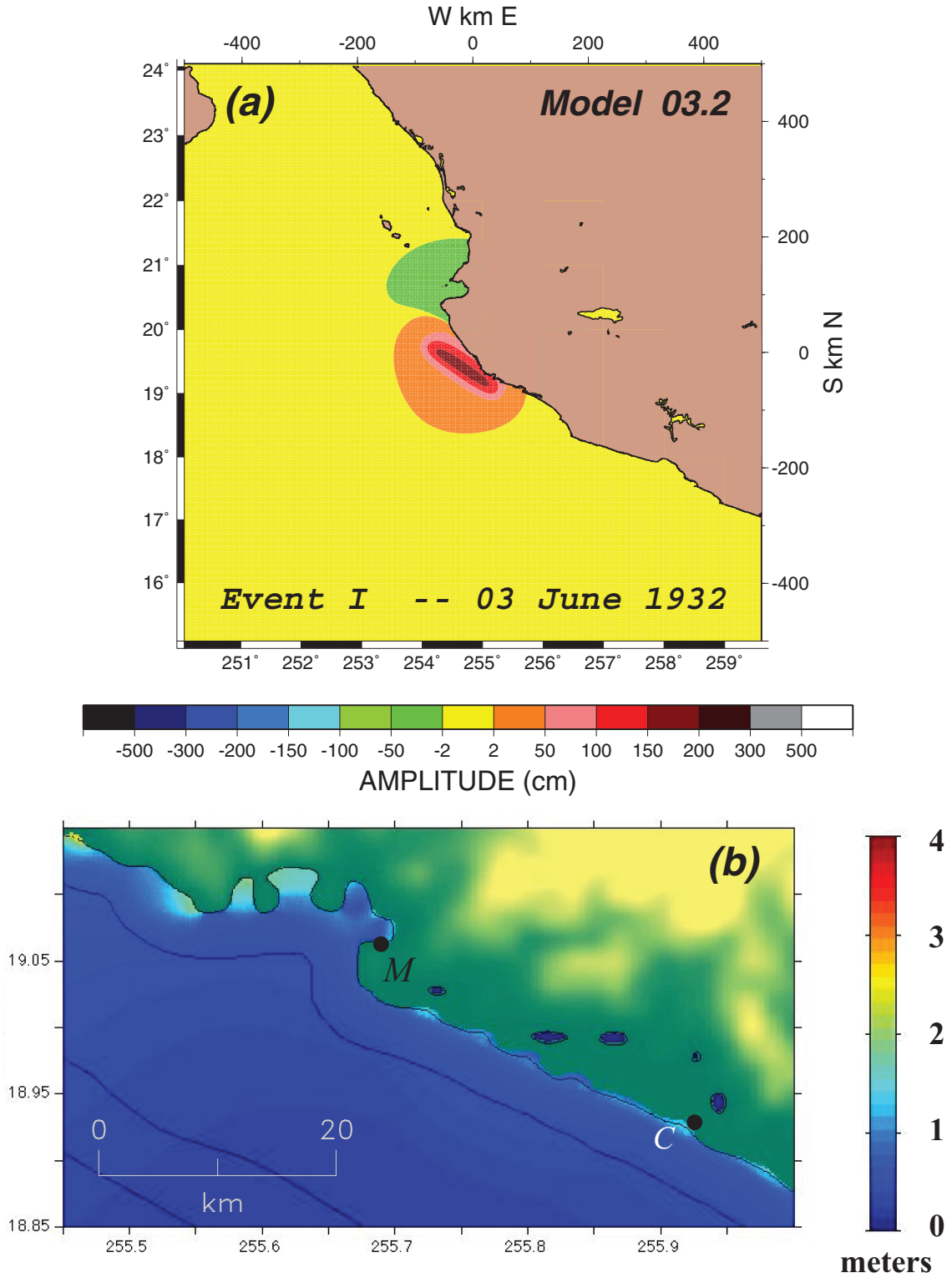

Figure 7. Same as Fig. 6 for Model 03.2. Note significantly lower wave heights.

surveyed), namely 10 m (Sánchez & Farreras 1993), remains less than twice the modelled slip on the fault ($\Delta u = 6.5$ m) under Model 22.4, which satisfies the 'Plafker rule of thumb' (Okal & Synolakis 2004) and confirms that the tsunami can be explained satisfactorily without the need of an ancillary source such as an underwater landslide.

6 DISCUSSION AND CONCLUSIONS

A detailed seismological study of the 1932 sequence in Manzanillo and in particular of Events I, II and III, confirms that the latter occurred up-dip of the main shock and that it featured source slowness resulting in a growth of moment with period and in a deficiency of high frequencies in its source spectrum. Event III is a typical

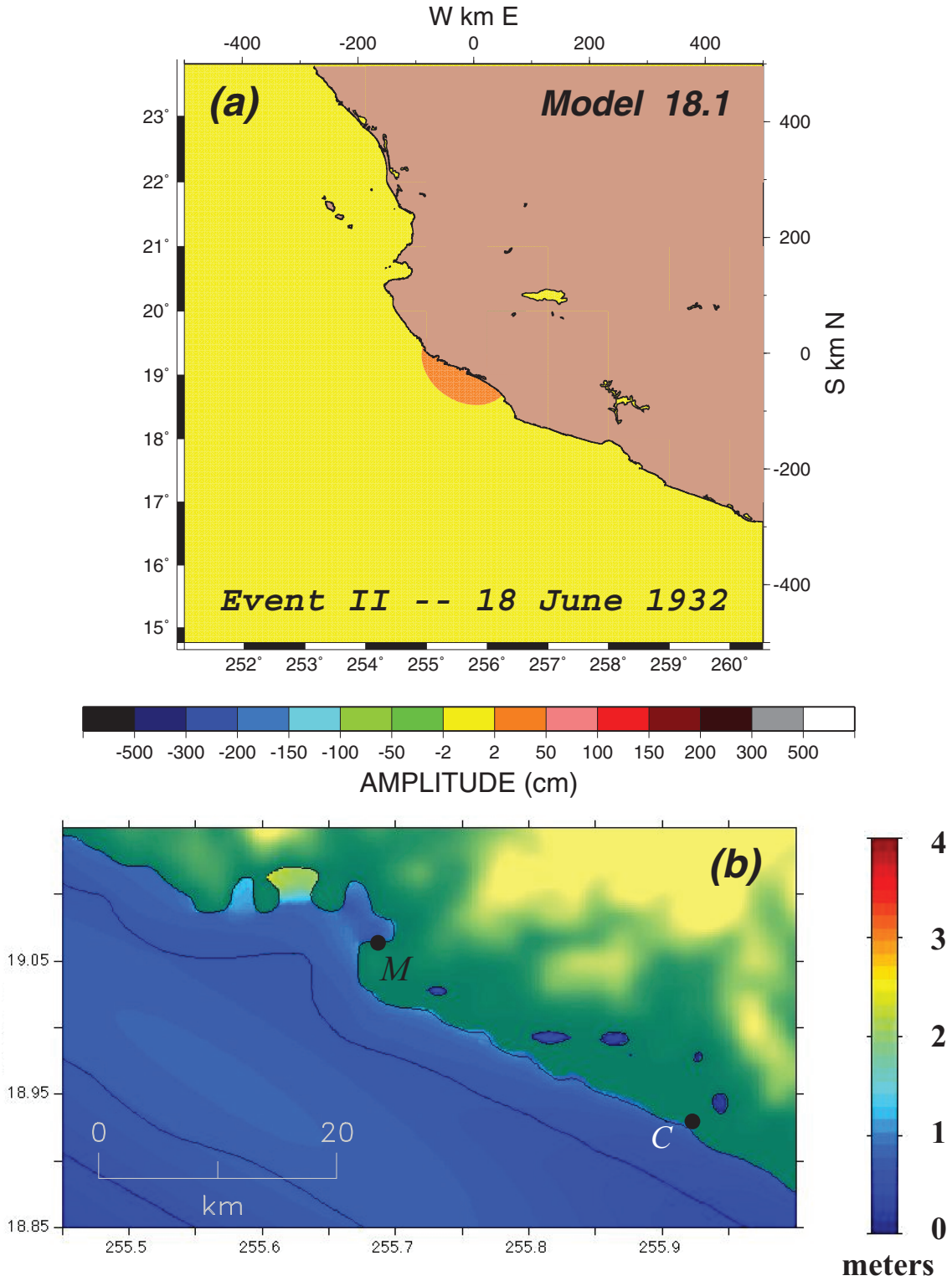

Figure 8. Same as Fig. 6 for Event II (Model 18.1). Note again significantly lower wave heights, in agreement with the weaker nature of the tsunami, as compared to Event I.

'tsunami earthquake', with a slowness parameter $\Theta = -6.18$, more than one logarithmic unit less than predicted by scaling laws.

Based on the long-period seismic moments derived in this study, our hydrodynamic simulations reproduce the main characteristic of the tsunamis as reported in historical chronicles: a run-up of about 3 m concentrated in the bay of Manzanillo during Event I, a much more benign tsunami during Event II and a catastrophic inundation after Event III with run-ups reaching 7 m; the latter is explained by setting the rupture on a splay fault in weaker, presumably sedimentary, material in the wedge of the subduction system under the exact

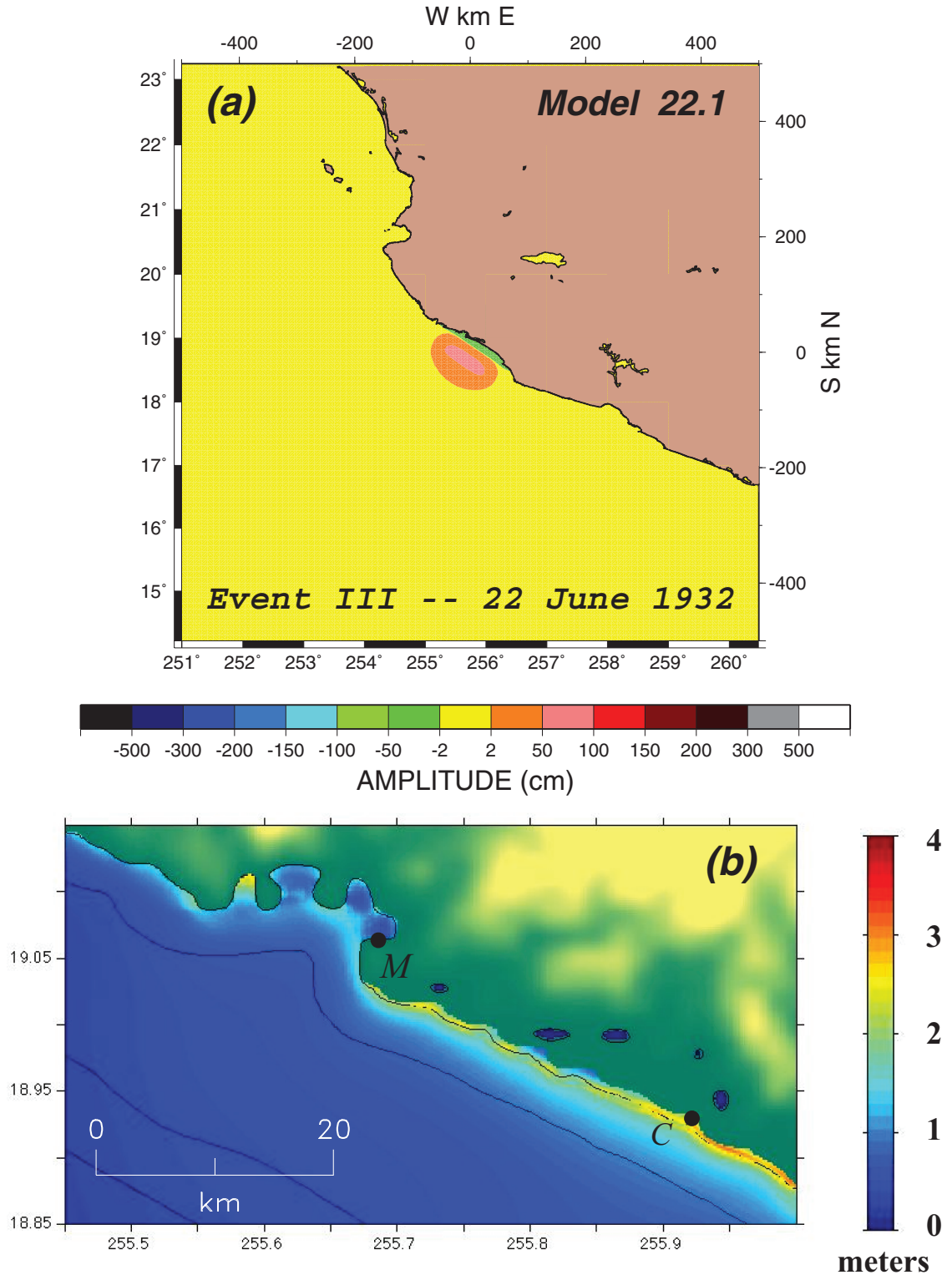

Figure 9. Same as Fig. 6 for Event III (Model 22.1). This model would predict a smaller, rather than larger, tsunami than for Event I.

scenario proposed by Fukao (1979) in the Kuril Islands. In particular, the catastrophic Event III tsunami can be modelled using the seismically anomalous source derived in Section 4, without the need to invoke a different mechanism such as an underwater landslide.

The 1932 Mexican sequence constitutes a classical example of a regular main shock triggering, within a few weeks' time, a slow 'tsunami earthquake'. In this respect, it is most reminiscent of the sequences of 1963 October and 1973–1975, both in the Kuril Islands. We show on Fig. 5 energy-to-moment ratios for the 'tsunami earthquakes' of 1963 October 20 ('K63') and 1975 June 10 ('K75') that were aftershocks of the regular subduction events of 1963 October 13 (Kanamori 1970) and 1973 June 17, respectively

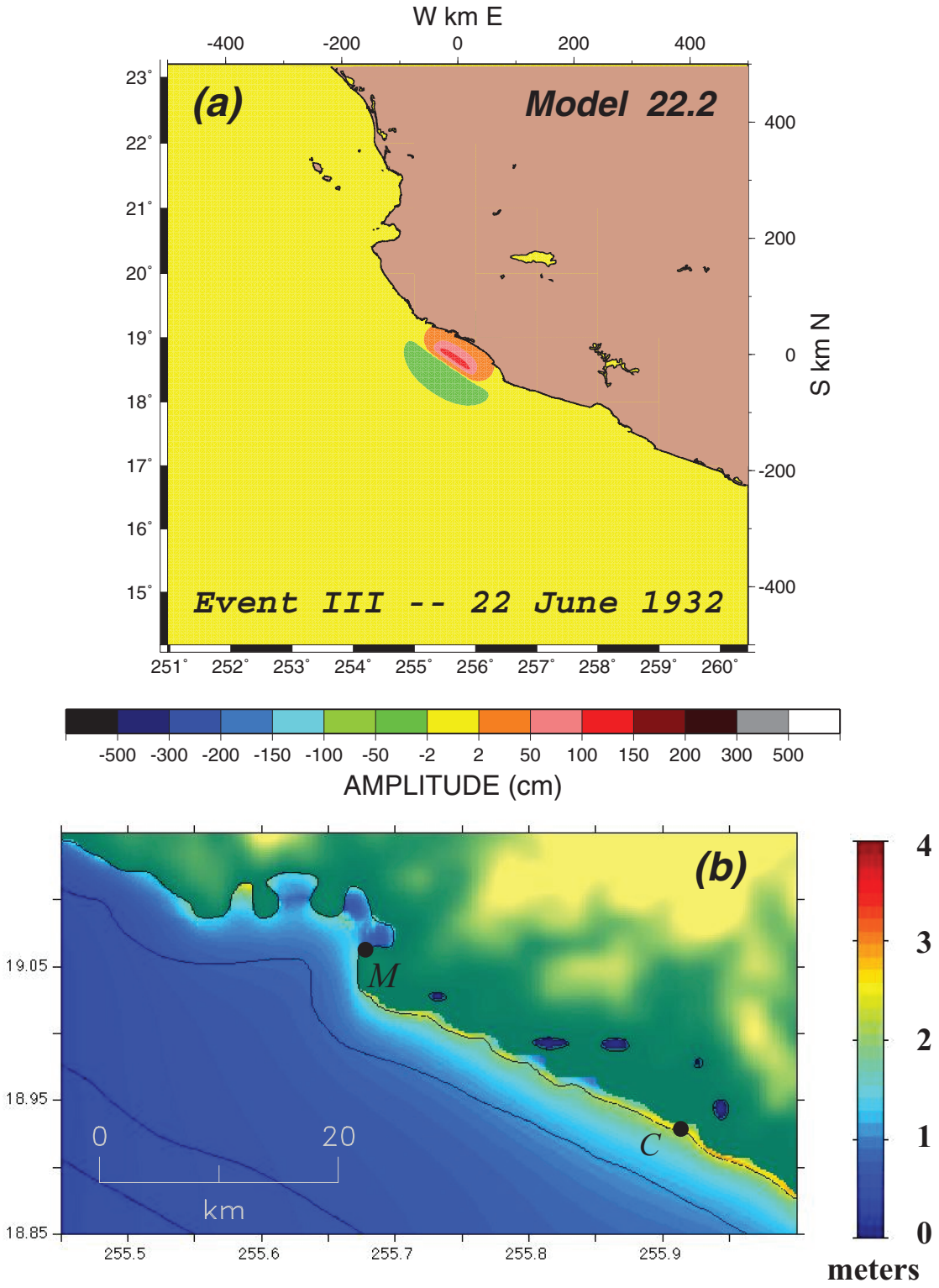

Figure 10. Same as Fig. 9 for Model 22.2, featuring a steeper fault dip. Although this model shows a marginal increase in wave heights, it still cannot account for the devastating nature of the tsunami.

(energy estimates were obtained from the Benioff 1–90 records of their *P* waves at Pasadena, and their moments were derived from WWSSN records of their mantle Love and Rayleigh waves). The resulting values of Θ (-6.37 and -6.43, respectively) are typical of recent tsunami earthquakes (e.g. Nicaragua, 1992, -6.47) and comparable to that derived for Event III. The similarity between the Kuril and Mexican sequences also extends to the moment ratios between the main shock and the 'tsunami earthquake', whose values (6.3 in 1932, 12.5 in 1963 and 7.5 in 1973–1975) are generally comparable.

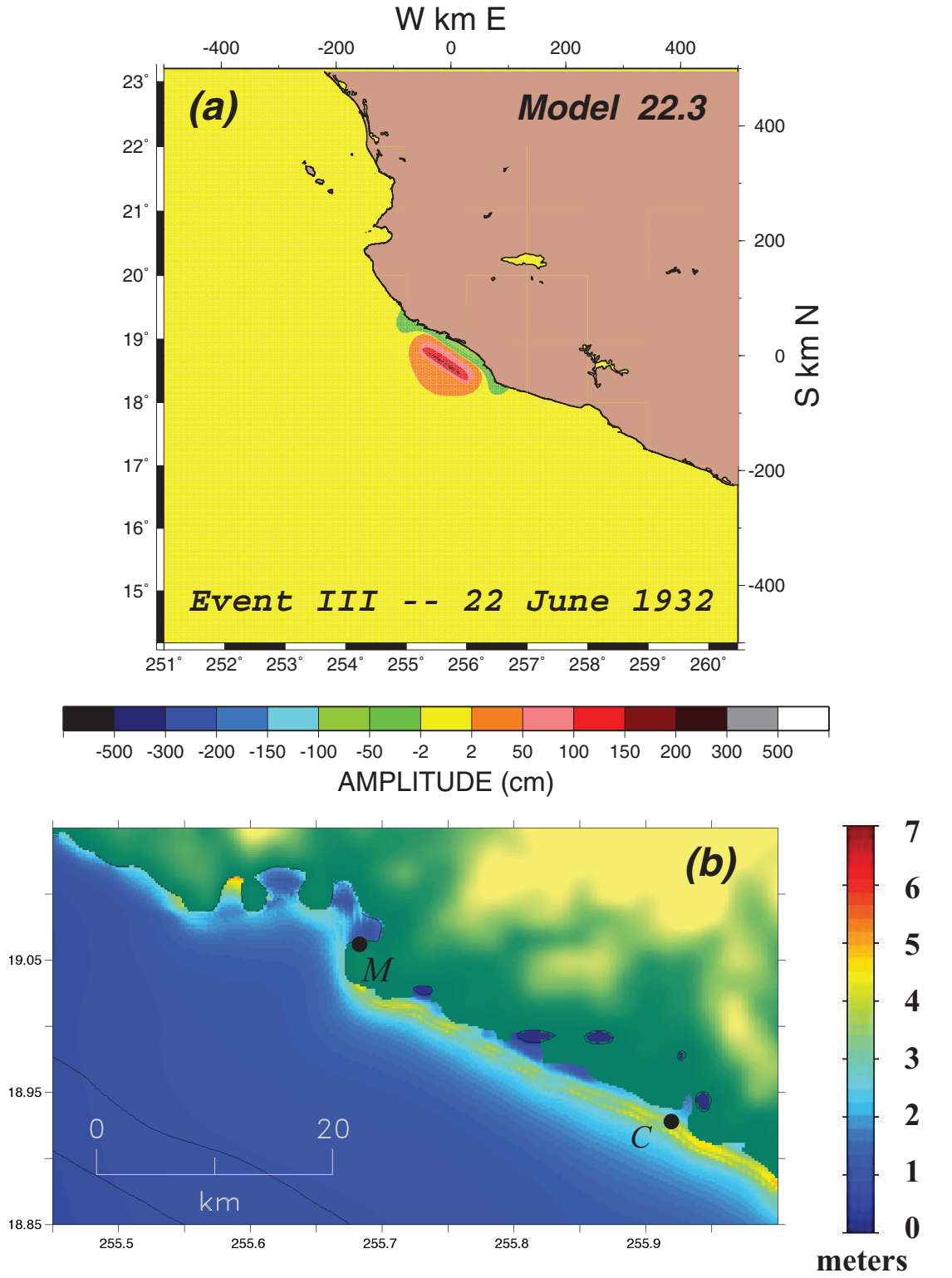

Figure 11. Same as Fig. 6 for Model 22.3, featuring a deficient rigidity along a gently dipping fault plane. Note the different scale of the palette in (b). Although this model produces larger waves than 22.1 and 22.2, they remain smaller than reported.

It is remarkable that Fukao's (1979) model, derived for the Kuril province, can be exported to a subduction zone with significantly different tectonic characteristics: a much younger age and a slower convergence rate. Following the occurrence of the 2004 Sumatra earthquake in a subduction zone where Ruff & Kanamori's (1980) paradigm did not predict a megathrust event, Stein and Okal (2007) cautioned that simple tectonic parameters were actually poor predictors of the occurrence of large earthquakes in subduction zones; the present results suggest that the same conclusion could apply to the triggering of 'tsunami earthquakes' after large subduction events. In

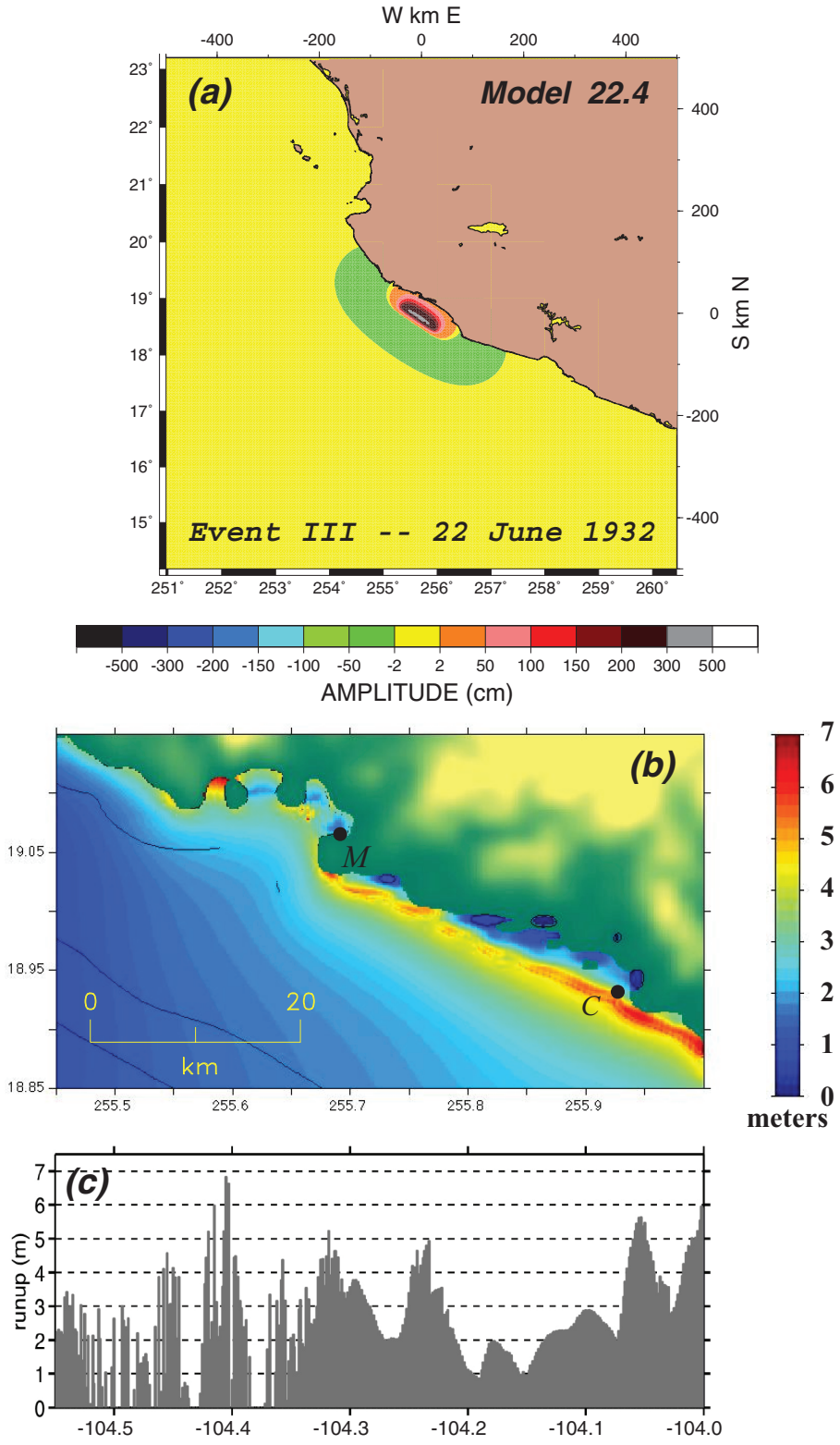

Figure 12. (a) and (b) Same as Fig. 9 for preferred Model 22.4, featuring rupture in a weaker material. The scale of the palette is common with Fig. 11, but differs from Figs 6–10. (c) Run-up along coastline, plotted as a function of longitude. Note inundation of Cuyutlán land spits and run-up reaching 7 m. See text for details.

this respect, the specific hazard inherent in those anomalous events that are treacherous because they do not carry the natural warning of an impending tsunami in the form of intense shaking, should be emphasized globally as part of tsunami education programs. Despite a slightly different mechanism that does not require rupturing on a splay fault (Newman *et al.* 2011), the recent Mentawai disaster (700 killed) illustrates the shortcomings of a natural warning relying only on shaking 'intensity', the challenges of educating

populations to the perception of shaking 'duration' remaining of course formidable (Fritz *et al.* 2011).

On the other hand, among the three sequences of Kuril-type tsunami earthquakes, the most variable parameter is the time delay between the main shock and the 'tsunami earthquake': 7 d in the 1963 episode, 19 d in 1932 but nearly 2 years in 1973–1975. (An additional element of diversity is the occurrence of many foreshocks including several large ones during the 1963 sequence.) An end-member to this series could be the 1896 Meiji Sanriku earthquake, for which Tanioka & Satake (1996) have argued that the rupture propagated coseismically into the accretionary wedge, with essentially no delay between the two events. This variability in delay before the 'tsunami earthquake' expresses the non-linear nature of the stress transfer outside of the rupturing area of the main shock. Obviously and unfortunately, the time delay in question would also be the most valuable parameter from a societal standpoint.

ACKNOWLEDGMENTS

We are grateful to Ota Kulhánek, James Dewey, Brian Mitchell and Bernard Dost for access to historical seismograms. Historical newspaper articles were compiled and translated in 2005 by Rachel Ryskin as part of an internship at Northwestern University. The paper was significantly improved by the comments of two anonymous reviewers.

REFERENCES

Ben-Menahem, A., 1961. Radiation of seismic surface waves from finite moving sources, *Bull. seism. Soc. Am.,* **51,** 401–435.

Bilek, S.L. & Lay, T., 1999. Rigidity variations with depth along interplate megathrust faults in subduction zones, *Nature,* **400,** 443–446.

Boatwright, J. & Choy, G.L., 1986. Teleseismic estimates of the energy radiated by shallow earthquakes, *J. geophys. Res.,* **91,** 2095–2112.

Courant, R., Friedrichs, K. & Lewy, H., 1928. Über die partiellen Differenzengleichungen der mathematischen Physik, *Math. Ann.,* **100,** 32–74.

Doser, D.I. & Webb, T.H., 2003. Source parameters of large historical (1917–1961) earthquakes, North Island, New Zealand, *Geophys. J. Int.,* **152,** 795–832.

Ebeling, C.W. & Okal, E.A., 2007. An extension to short distances of real-time estimators of seismic sources, *EOS, Trans. Am. geophys. Un.,* **88**(52) Abstract, S51C-01.

Eissler, H.K. & McNally, K.C., 1984. Seismicity and tectonics of the Rivera Plate and implications for the 1932 Jalisco, Mexico, earthquake, *J. geophys. Res.,* **89,** 4520–4530.

El Excelsior, Mexico, D.F., 23 de Junio de 1932.

Engdahl, E.R. & Villaseñor, A., 2002. Global seismicity: 1900–1999, in *International Earthquake and Engineering Seismology Part A*, pp. 665–690, eds, Lee, W.H.K., Kanamori, H., Jennings, P.C. & Kisslinger, C., Elsevier, New York, NY.

Espíndola, J.M., Singh, S.K., Yamamoto, J. & Havskov, J., 1981. Seismic moments of large Mexican subduction earthquakes since 1907, *EOS, Trans. Am. geophys. Un.,* **62,** 948 [Abstract].

Fritz, H.M., Borrero, J.C., Suwargadi, B., Lin, L., Qiang, Q., Pranantyo, I.R., Skanavis, V. & Synolakis, C.E., 2011. Reconnaissance of the 25 October 2010 Mentawai Islands tsunami in Indonesia, *Geophys. Res. Abstr.,* **13,** EGU2011–9512.

Fukao, Y., 1979. Tsunami earthquakes and subduction processes near deep-sea trenches, *J. geophys. Res.,* **84,** 2303–2314.

Geller, R.J., 1976. Scaling relations for earthquake source parameters and magnitudes, *Bull. seism. Soc. Am.,* **66**, 1501–1523.

Godunov, S.K., 1959. Finite difference methods for numerical computations of discontinuous solutions of the equations of fluid dynamics, *Mat. Sb.,* **47,** 271–295.

Goodstein, J.R., Kanamori, H. & Lee, W.H.K., 1980. Seismology microfiche publications from the Caltech archives, *Bull. seism. Soc. Am.,* **70,** 657–658.

Gutenberg, B. & Richter, C.F., 1954. *Seismicity of the Earth and Associated Phenomena*, Princeton University Press, Princeton, NJ, 310pp.

Heezen, B.C. & Ewing, W.M., 1952. Turbidity currents and submarine slumps, and the 1929 Grand Banks earthquake, *Am. J. Sci.,* **250,** 849–878.

Kanamori, H., 1970. Synthesis of long-period surface waves and its application to earthquake source studies – Kuril Islands earthquake of October 13, 1963, *J. geophys. Res.,* **75,** 5011–5027.

Kanamori, H., 1972. Mechanism of tsunami earthquakes, *Phys. Earth planet. Inter.,* **6,** 346–359.

Lay, T. & Bilek, S.L., 2007. Anomalous earthquake ruptures at shallow depths on subduction zone megathrusts, in *The Seismogenic Zone of Subduction Thrust Faults*, pp. 476–511, eds Dixon, T. & Moore, C., Columbia Univ. Press, New York, NY.

López, A.M. & Okal, E.A., 2006. A seismological reassessment of the source of the 1946 Aleutian "tsunami" earthquake, *Geophys. J. Int.,* **165,** 835–849.

Mansinha, L. & Smylie, D.E., 1971. The displacement fields of inclined faults, *Bull. seism. Soc. Am.,* **61,** 1433–1440.

Newman, A.V. & Okal, E.A., 1998. Teleseismic estimates of radiated seismic energy: the E/M_0 discriminant for tsunami earthquakes, *J. geophys. Res.,* **103,** 26 885–26 898.

Newman, A.V., Hayes, G., Wei, Y. & Convers, J., 2011. The 25 October 2010 Mentawai tsunami earthquake, from real-time discriminants, fault rupture, and tsunami excitation, *Geophys. Res. Lett.,* **38**(5), **7**, L05302, doi:10.1029/2010GL046498.

Okal, E.A., 1988. Seismic parameters controlling far-field tsunami amplitudes: a review, *Nat. Hazards,* **1,** 67–96.

Okal, E.A., 1992. Use of the mantle magnitude $M_{\rm m}$ for the reassessment of the seismic moment of historical earthquakes. I: shallow events, *Pure appl. Geophys.,* **139,** 17–57.

Okal, E.A. & Kirby, S.H., 2002. Energy-to-moment ratios for damaging intraslab earthquakes: preliminary results on a few case studies. *USGS Open File Rept.* **02–328**, 127–131.

Okal, E.A. & Reymond, D., 2003. The mechanism of the great Banda Sea earthquake of 01 February 1938: applying the method of preliminary determination of focal mechanism to a historical event, *Earth planet. Sci. Lett.,* **216,** 1–15.

Okal, E.A. & Synolakis, C.E., 2003. Theoretical comparison of tsunamis from dislocations and landslides, *Pure appl. Geophys.,* **160,** 2177–2188.

Okal, E.A. & Synolakis, C.E., 2004. Source discriminants for near-field tsunamis, *Geophys. J. Int.,* **158,** 899–912.

Okal, E.A. & Talandier, J., 1989. M_m: a variable period mantle magnitude, *J. geophys. Res.,* **94,** 4169–4193.

Okal, E.A., Hongsresawat, S. & Stein, S., 2011. Split mode evidence for no ultra-slow component to the source of the 2010 Maule, Chile earthquake, *Bull. seism. Soc. Am.*, in press.

Polet, J. & Kanamori, H., 2000. Shallow subduction zone earthquakes and their tsunamigenic potential, *Geophys. J. Int.,* **142,** 684–702.

Reid, I.D., 1976. The Rivera plate: a study in seismology and tectonics, *PhD thesis*, Univ. California, San Diego.

Repetti, W.C., 1934. The China Sea earthquake of February 14th, 1934, in *Seismological Bulletin for 1934 January-June, Dept. Agriculture & Commerce*, pp. 22–29, Govt. of the Philippine Is., Manila.

Richter, C.F., 1958. *Elementary Seismology*, W.H. Freeman, San Francisco, CA, 768pp.

Ruff, L.J. & Kanamori, H., 1980. Seismicity and the subduction process, *Phys. Earth planet. Inter.,* **23,** 240–252.

Sánchez. D., A.J., and S.F. Farreras, S., 1993. Catálogo de tsunamis (Maremotos) en la Costa Occidental de Mexico [Catalog of tsunamis on the Western coast of Mexico], World Data Center A Pub. SE-50, U.S. Dept. of Commerce, Boulder, CO, 79pp.

Satake, K., *et al*., 1993. Tsunami field survey of the 1992 Nicaragua earthquake, *EOS, Trans. Am. geophys. Un.,* **74,** 145 and 156–157.

Singh, S.K., Domínguez, T., Castro, R. & Rodríguez, M., 1984. *P* waveform of large, shallow earthquakes along the Mexican subduction zone, *Bull. seism. Soc. Am.,* **74,** 2135–2156.

Singh, S.K., Ponce, L., & Nishenko, S., 1985. The great Jalisco, Mexico, earthquakes of 1932: subduction of the Rivera plate, *Bull. seism. Soc. Am.,* **75,** 1301–1313.

Stein, S. & Okal, E.A., 2007. Ultra-long period seismic study of the December 2004 Indian Ocean earthquake and implications for regional tectonics and the subduction process, *Bull. seism. Soc. Am.,* **97,** S279–S295.

Synolakis, C.E., 2003. Tsunami and seiche, in *Earthquake Engineering Handbook*, pp. 9-1– 9-90, eds Chen, W.-F. & Scawthron, C., CRC Press, Boca Raton, FL.

Synolakis, C.E., Bardet, J.-P., Borrero, J.C., Davies, H.L., Okal, E.A., Silver, E.A., Sweet, S. & Tappin, D.R., 2002. The slump origin of the 1998 Papua New Guinea tsunami, *Proc. Roy. Soc. (London), Ser. A.*, **458,** 763–789.

Talandier, J. & Okal, E.A., 1989. An algorithm for automated tsunami warning in French Polynesia, based on mantle magnitudes, *Bull. seism. Soc. Am.,* **79,** 1177–1193.

Tanioka, Y. & Satake, K., 1996. Fault parameters of the 1896 Sanriku tsunami earthquake estimated from tsunami numerical modeling, *Geophys. Res. Lett.,* **23,** 1549–1552.

Tanioka, Y., Ruff, L.J. & Satake, K., 1997. What controls the lateral variation of large earthquake occurrence along the Japan trench? *Island Arc,* **6,** 261–266.

Taylor, F.W., Briggs, R.W., Frohlich, C., Brown, A., Hornbach, M., Papabatu, A.K., Meltzner, A. & Billy, D., 2008. Rupture across arc segment and plate boundaries in the 1 April 2007 Solomons earthquake, *Nat. Geosci.,* **1,** 253–257.

Titov, V.V. & Synolakis, C.E., 1998. Numerical modeling of tidal wave runup, *J. Waterw. Port Coast. Ocean Eng.,* **B124,** 157–171.

Wang, S.-C., McNally, K.C. & Geller, R.J., 1982. Seismic strain release along the Middle America Trench, Mexico, *Geophys. Res. Lett.,* **9,** 182–185.

Wysession, M.E., Okal, E.A. & Miller, K.L., 1991. Intraplate seismicity of the Pacific Basin, 1913–1988, *Pure appl. Geophys.,* **135,** 261–359.

Yagi, Y., Mikumo, T., Pacheco, J. & Reyes, G., 2004. Source rupture process of the Tecoman, Colima, Mexico earthquake of January 22, 2003, determined by joint inversion of teleseismic body wave and near source data, *Bull. seism. Soc. Am.,* **94,** 1795–1807.